Research Article | Vol. 13, No. 1 / 1 Jan 2022 / Biomedical Optics Express 93
Biomedical Optics EXPRESS

Temperature dependent terahertz spectroscopy and imaging of orthotopic brain gliomas in mouse models

LIMIN WU,[1,2] YUYE WANG,[1,2,4] BIN LIAO,[3] LU ZHAO,[3] KAI CHEN,[1,2] MEILAN GE,[1,2] HAIBIN LI,[1,2] TUNAN CHEN,[3] HUA FENG,[3] DEGANG XU,[1,2,5] AND JIANQUAN YAO[1,2]

[1]*Institute of Laser and Optoelectronics, School of Precision Instruments and Optoelectronics Engineering, Tianjin University, Tianjin 300072, China*
[2]*Key Laboratory of Optoelectronic Information Science and Technology (Ministry of Education), Tianjin University, Tianjin 300072, China*
[3]*Department of Neurosurgery and Key Laboratory of Neurotrauma, Southwest Hospital, Third Military Medical University (Army Medical University), Chongqing 400038, China*
[4]*yuyewang@tju.edu.cn*
[5]*xudegang@tju.edu.cn*

Abstract: Terahertz (THz) spectroscopy and imaging were used to differentiate brain gliomas in a mouse model at different temperatures. The THz spectral difference between brain glioma and normal brain tissues at -10°C and 20°C was obtained in the 0.4–2.53 THz range. The absorption coefficient and refractive index values varied with both temperature and frequency. The fresh ex vivo brain glioma tissues were mapped by THz attenuated total reflection (ATR) imaging at 2.52 THz in the temperature range from -20°C to 35°C. Compared with histological examination, THz-ATR imaging could better display the tumor areas at a higher temperature. And the averaged reflectivity of normal tissue was increased with the increase of temperature, whereas the tumor region showed a decreasing trend. Thus, the larger THz imaging difference between glioma and normal tissues could be obtained. Moreover, *in vivo* brain gliomas in mice models could also be differentiated clearly from normal brain tissues using THz-ATR imaging at 2.52 THz under room temperature. The THz-ATR images corresponded well with those of visual and hematoxylin and eosin (H&E) stained images. Therefore, this pilot study demonstrated that temperature dependence THz spectroscopy and imaging are helpful to the brain gliomas in mouse model detection.

© 2021 Optica Publishing Group under the terms of the Optica Open Access Publishing Agreement

1. Introduction

Terahertz (THz) wave, referring to the electromagnetic wave with the frequency range of 0.1 - 10 THz, lies between infrared and microwave regions [1]. Based on its characteristics of non-ionization, fingerprint spectrum, and water sensitivity, THz technology has been utilized in various applications such as chemical recognition, security inspection, pharmaceutical testing, and medical imaging [2,3]. In recent years, THz spectroscopy and imaging have been utilized in various types of cancer detection such as skin, breast, colon, and liver cancers [4–7]. Previous studies have provided preliminary experimental evidence that THz spectroscopy and imaging can be able to identify lesion tissues.

Gliomas are the most common primary intracranial tumors. It grows invasively and has unclear margins between the neoplastic and normal regions [8]. Even experienced surgeons cannot increase the rate of complete resection beyond 20% using white light microscopy [9]. THz spectra and imaging have been used to reveal essential characteristics differences between tumor and normal tissues. The results demonstrated that paraffin-embedded [10–12] and freshly-excised

#445597 https://doi.org/10.1364/BOE.445597
Journal © 2022 Received 11 Oct 2021; revised 21 Nov 2021; accepted 29 Nov 2021; published 6 Dec 2021

Biomedical Optics EXPRESS

[11–15] *ex vivo* brain tumors from rat, *ex vivo* [16,17]and *in vivo* [17,18] brain gliomas from mice, and even the snap-frozen [19] and freshly-excised human brain [20,21] could be differentiated clearly from normal brain tissues. Especially, THz imaging for the intraoperative label-free discrimination between intact tissues and glioma was highlighted compared with the common modalities of the brain imaging [13]. The refractive index and absorption coefficients of tumor regions were higher than normal tissues, because glioma regions have the presence of increased water content, nuclear atypia, mitotic activity and florid microvascular proliferation than that in normal region [22]. In addition, Yamaguchi et al. quantitatively described water content and cell density were the origin of differences in the refractive index between normal and tumor tissues using THz spectroscopy [12]. Gavdush et al. developed relaxation models of complex dielectric permittivity to analyze the *ex vivo* intact tissues and WHO grade I–IV gliomas of the human brain [21]. However, the difference of THz wave optical parameters between glioma and normal tissues were all small.

To improve the difference between normal and tumor tissues in THz band for better recognizing tumor region, much work has been done. The reflectance difference between normal and cancerous tissues was enlarged using continuous wave THz polarization imaging, but this method will cause extreme energy loss [23]. Signal analysis methods with suitable parameters were proposed to improve the detection sensitivity, such as interference elimination algorithm [24], feature extraction algorithm [25,26], and spectroscopic integration technique. Thus, the response time of THz detector should be considered and a lot of sample test data were necessary. Considering water content was one of the key factors for discriminating tumor tissue from normal tissue, frozen tissue and nanoparticle probe were used to improve the detection difference. However, nanoparticle probe [27] not only caused the burden on the patient but also sometimes would stain normal tissues around the tumor. Png et al. found some distinction in the THz absorption spectra of healthy and diseased snap-frozen human brain tissues for the first time [19]. Then, THz signal gap between the healthy and completely metastatic lymph nodes [28] and better contrast in THz spectroscopic image of frozen excised oral malignant melanoma [29] and excised oral cancer [30] at -20°C were also found. In addition, Zotov et al. even demonstrated experimentally the ability of THz pulsed spectroscopy for in situ monitoring of tissue freezing depth in the tissue cryosurgery. Processing of THz pulsed signal within 45 s demonstrated the ability to detect the movement of freezing front up to the depth of 657 μm [31]. These results indicated that the physical properties (THz dielectric properties) of biological tissues were closely related to the temperature in THz frequency range. In other words, the sample temperature has important effect on THz detection of diseased tissue. However, there is no report about temperature dependence on THz measurement of brain glioma.

In this paper, the discriminability of freshly *ex vivo* brain glioma samples at different temperatures were investigated, using the THz spectroscopy and imaging. The results showed that the better contrast of THz measurement of brain glioma can be obtained at higher temperature. Furthermore, glioma regions of *in vivo* mice brain tissues could be differentiated clearly using THz-ATR imaging system at room temperature, which were similar to those of the corresponding visual and H&E-stained images.

2. Methods

2.1. Experimental setup

To investigate the THz spectrum characteristic of brain tissues, the commercially available THz-TDS (Advantest Corp., TAS7500SP) worked in the transmission geometry was used. The spectrum reached 4.0 THz from 0.1 THz, with the frequency resolution of 7.6 GHz and the spatial resolution of 2 mm. The sample was installed at the focal point of THz time domain spectrometer. Usually, biological tissue with high THz wave absorption was cut into slices with a certain thickness, which was sandwiched by a pair of quartz windows. The windows were

Biomedical Optics EXPRESS

attached to a copper sheet with the semiconductor cooling sheet and cooling water circulation. The temperature of a copper sheet was monitored using the resistance temperature sensor. The temperature float was controlled within ± 1°C. The measurements were performed at different temperature (-10°C and 20°C) with dry air purge. Considering the time delay of temperature control system, spectral measurement was performed after setting the temperature for 5 minutes.

Our home-made continuous-wave THz-ATR imaging system was used in this paper [16], as shown in Fig. 1. An optically pumped THz gas laser (FIRL 100, Edinburgh Instruments Ltd.) was used, which was capable of emitting high-power, tunable continuous THz wave. The maximum THz output power was up to 150 mW at 2.52 THz. THz wave was separated into two beams by wire-grid beam splitter (Micromesh Instruments, Inc.). One beam served as the intensity reference to improve the SNR of THz imaging and the other beam was used as signal. The reference light was directly detected by a Golay cell (GC-1P, Tydex Ltd.), whereas the signal light was collimated and focused by four off-axis parabolic mirrors (F = 1 and f = 2 inch), reached another Golay cell after reflection from the sample positioned in the THz beam path. An isosceles triangle shaped silicon prism ($n = 3.42$ @ 2.52 THz) with base angle of 49° placed over the sample with contact pressure for imaging. Here, the sample was located at the focus of the THz beam. The value of incident angle at the sampling surface was 43.5° and this incident angle was larger than the theoretical critical angle of 37.5° for distilled water. In addition, temperature control device was also adopted to control sample temperature (-20°C - 35°C) in this imaging system, which was the same as that used in the THz-TDS. Unlike in spectrum system, the sample was placed on a copper sheet and its upper surface was in close contact with the bottom surface (34.8×34.8 mm^2) of prism for THz-ATR imaging, which was mounted on a two dimensional (2D) movable sample stage (SIGMA KOKI CO., LTD.). The scanning step in this study was set as 200 μm and the resolution was 450 μm × 500 μm [16,32].

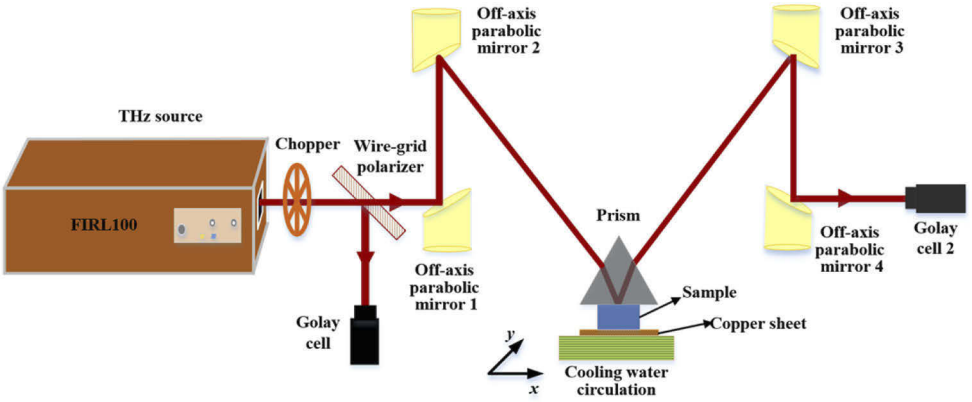

Fig. 1. Continuous-wave THz-ATR imaging system.

2.2. Sample preparation

An orthotopic glioma model for mouse was used as the brain glioma model and this model has a clear boundary between normal and tumor tissues. A total of 18 BALB/c Male nude mice (3~4 weeks) were purchased from Beijing Hua Fu Kang Biotechnology Limited Liability Company (Beijing HFK Bio-Technology.co., LTD). U87-MG cell line was obtained from American Type Culture Collection (ATCC, Manassas, Virginia). All animal experiments were performed in accordance with the China Animal Welfare Legislation, and were approved by the Third Military Medical University Committee on Ethics for the Care and Use of Laboratory Animals.

Biomedical Optics EXPRESS

The samples were divided into three groups and used for the spectrum measurement of freshly excised brain tissues, freshly excised brain tissues imaging and *in vivo* imaging. The number of samples with glioma in each group is 5. The glioma model was established by surgically implanting U87-MG cells into mouse. For the comparison, the same surgical procedures were also performed on the normal mice. Detailed experimental procedures have been reported in our published paper [17]. The mice were all allowed to grow for 2-3 weeks. For the samples of spectroscopy and *ex vivo* imaging measurement, the mice were directly euthanized and their brains were removed immediately prior to THz measurements. The extracted brains were divided evenly on the coronal surface with a scalpel. One part was for THz imaging or spectrum measurement and the other part was quickly put to -15°C slicing machine for freezing slice staining. For spectrum measurement, in order to avoid water loss and other errors during sample measurement, the tissue with 60μm thickness was sandwiched by two quartz plates (0.5 mm thickness) and wrapped with vaseline and oleic acid. For the sample of *in vivo* imaging, a cranial window was made to expose the brain tumor. The surrounded blood and cerebrospinal fluid were sucked away by brain cotton slices. The *in vivo* sample was in close contact with the attenuated total reflection prism to obtain THz-ATR image. Although such process causes some shift or extrusion for local tissue less than 1 mm, it is acceptable in neurosurgical operations. Then, the mice were euthanized and their entire brains were removed immediately. The freshly excised brain tissues were quickly put to -15°C slicing machine, and a thin section of 20 μm thickness was sliced from the surface for histopathological examination by H&E staining.

2.3. Data analysis

For spectrum measurement, when the THz wave propagates from the THz emitter to the detector, THz electric field signals with and without samples (denoted by E_{sam} and E_{ref} respectively) are obtained. The effect of quartz window reflection can be ignored by selecting the THz time-domain pulse delay signal caused by sample. Further, the frequency domain signals can be obtained through the Fourier transform, which are expressed as [10],

$$E_{ref}(\omega) = E_0(\omega)\exp(-i\omega t + i\frac{\omega}{c}l) \tag{1}$$

$$\begin{aligned} E_{sam}(\omega) = E_0(\omega)(\frac{2}{N(\omega)+1})\exp\left[-i\omega t + i\frac{n(\omega)\omega}{c}d + i\frac{\omega}{c}(l-d)\right] \\ \times \exp\left[-\frac{\kappa(\omega)}{c}d\right]\frac{2N(\omega)}{N(\omega)+1} \\ \times \sum_{k=0}^{\infty}\left\{\left[\frac{N(\omega)-1}{N(\omega)+1}\right]^2 \cdot \exp\left[i\frac{2n(\omega)\omega}{c}d - \frac{2\kappa(\omega)}{c}d\right]\right\}^k \end{aligned} \tag{2}$$

Here, E_0 is the original THz pulse emitted by the photoconductive antenna, ω is the frequency of THz wave, l is the full path that the THz wave travels, d is the thickness of the sample, and $N(\omega) = n(\omega) + i\kappa(\omega)$ is the complex refraction of measured sample, in which $n(\omega)$ is the refractive index, and $\kappa(\omega)$ is the extinction coefficient. k is the number of reflections, and k=0 is used in this study. To calculate refractive index and extinction coefficient of the biosample, $E_{\mathrm{sam}}(\omega)/E_{\mathrm{ref}}(\omega)$ should be performed. In addition, the absorption coefficient α can be calculated by the equation $\alpha(\omega) = 2\kappa(\omega)/c$.

For imaging, based on both quartz and silicon prism windows have high transmittance in the THz band, we ignored the reflected THz intensity caused by the marginal Fresnel loss due to their different refractive indices. The spectral data used in this study was constructed from 5 glioma model mice. The time-domain THz pulses were collected at three different spots in tumor area or healthy area for each sample. Every measurement point was repeatedly tested 3 times

Biomedical Optics EXPRESS

with the setting of 1024 times scan for each measurement. Due to the biological diversity, all spectra are averaged results of 15 measurement times and the standard deviation is shown as error bars. THz imaging with and without sample were measured as the images of F_{sample} and $F_{\text{substrate}}$, respectively. Considering the uniformity of the silicon prism, $F_{\text{substrate}}$ was taken as the image reference for simplicity. Thus, the reflectivity (R_r) of sample can be calculated by dividing the pixel values in $F_{\text{substrate}}$ by F_{sample}. Similarly, the reflectivity of silicon prism is obtained by using the air as the reference. The averaged reflectivity (R_{ave}) is defined as the average of multiple pixels within the regions of interest and statistical analyses were conducted by calculating the values of R_{ave}.

3. Results and discussions

3.1. THz spectroscopy of freshly excised brain tissues

First, we measured freshly excised mice brain tissues by THz-TDS system. Total 5 mice brain glioma models were used in spectral measurement. The whole brain extracted from mouse was cut in half. One part was for spectral measurement and the other was used for pathologically determined with the H&E-stained image. Considering the spatial resolution of spectral system is about 2 mm, the samples used in spectral measurement were horizontally sliced to ensure that the THz spot was located in the region of the tumor region. Figure 2 (a) show the examples of visual image of measured samples (NO. 1 and NO. 2), whereas Fig. 2 (b) show the H&E-stained images for freshly excised brain tissues. The tumor regions appeared paler in the visible images of frozen samples, which were marked by dashed lines in Fig. 2 (a). The region-stained deep purple was tumor region. This indicated cell density in tumor region was greater than those at the normal tissue [17]. The tumor areas of samples used in spectral measurement were all larger than 5×5 mm^2, as shown in Fig. 2 (b). The time-domain THz pulses were collected in normal and tumor regions for each sample, as points A and B shown in the Fig. 2 (a), respectively.

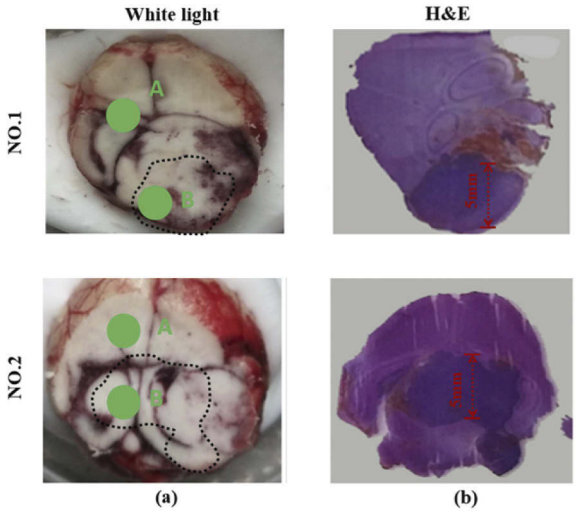

Fig. 2. (a) visual and (b) H&E-stained images of freshly excised brain glioma model.

Figure 3 (a) and Fig. 3 (b) show the refractive index spectra and the absorption coefficient spectra of freshly excised brain tissues at -10°C (frozen temperature) and 20°C (close to room temperature), respectively. On the whole, the average values of refractive index and absorption in normal tissues were both smaller than that in tumor tissue at two temperatures in the range from 0.4 THz to 2.53 THz. The increase of water content in the tumor region was the dominant reason

Biomedical Optics EXPRESS

for the difference [33], which would affect the refractive index and absorption coefficient of tissue [12,34]. In addition, it was clearly seen that the refractive index and absorption coefficient of brain tissue at 20℃ was higher than that at -10℃. The inset of Fig. 3 (a) and Fig. 3 (b) show the difference values of refractive index and absorption coefficient between tumor and normal tissues at different temperature. From the inset of Fig. 3 (a), the difference of refractive index for tumor and normal tissues showed a slight increase at higher temperature. This result was consistent with that of previous papers [29,30]. Moreover, the difference values of refractive index display an increasing trend for higher THz frequency. From the inset of Fig. 3 (b), the difference of THz absorption coefficients between normal and tumor tissues at 20℃ and -10℃ was significantly different in the 0.5-2.53 THz range. Therefore, it is necessary to select the best detection temperature for THz imaging. Moreover, the refractive index and absorption coefficient both are the important factors for the ATR imaging. Considering the ATR reflectivity variation caused by refractive index change is larger than that caused by absorption coefficient change, higher THz frequency is preferred for the study of temperature dependent THz imaging. Additionally, it is mentioned that the absorption coefficient curves in Fig. 3(b) seemed distorted in THz frequency domain. It might attribute to that water content and cell components shows different THz responses at different THz frequency, especially the tissue morphology including hydration state changes from -10℃ to 20℃.

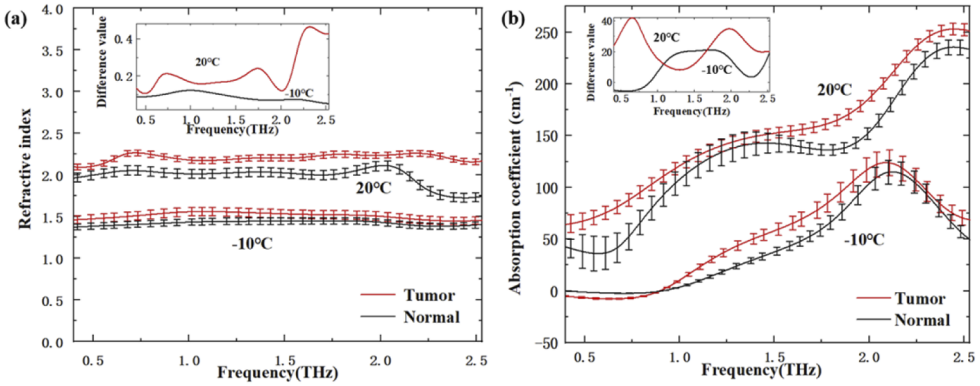

Fig. 3. (a) refractive index and (b) absorption coefficient of tumor and normal tissues under different temperature, the insets of (a) and (b) show the difference of the refractive index and the absorption coefficient between tumor and normal tissue, respectively.

3.2. THz imaging of freshly excised brain tissues

Then, in order to accurately evaluate the temperature effect on the THz imaging of brain glioma tissue, a homemade continuous-wave THz-ATR imaging system with 2.52 THz was used to measure the total of 5 freshly excised brain tissue samples with glioma at temperature from -20℃ (frozen temperature) to 35℃ (close to body temperature) at intervals of 5℃.

Figure 4 shows the visual, H&E-stained, and THz-ATR images for freshly excised brain tissues examples (NO. 3 and NO. 4). The whole brain extracted from mouse was cut into half. One part was for imaging measurement and the other was used for pathologically determined. Figure 4 (a) and (d) show the whole brain divided evenly on the coronal surface with a scalpel. The brightness regions in the visual image were tumor region, which were marked by dashed lines. The H&E-stained images were shown in Fig. 4 (b) and (e). Figure 4 (c) and (f) show the THz-ATR images of brain glioma samples at different temperatures of -20℃, -10℃, 0℃, 10℃ and 35℃, where the pixels were represented using the relative reflectivity (R_r) and lower R_r means the larger sample absorption. The THz high absorption region was the tumor region,

Biomedical Optics EXPRESS

which could be distinguished clearly from the normal tissues. However, the THz images of brain glioma at different temperature depicted obvious difference, where the stronger THz-wave absorption occurred at higher temperature. Furthermore, the average reflectance (56%±5%) of normal tissues was used as a comparison we estimated image size of the tumor detected by THz-ATR images for NO. 3 and NO. 4 samples, as listed in the Table 1. Especially, the tumor size indicated by H&E-staining was used as gold standard as comparison. The tumor regions areas shown in the THz images at $T = 35$℃ were similar to that of the corresponding H&E-stained image. Generally, considering the tumor cells grow invasively and proliferate, the water content of the tumor region was increased because angiogenesis occurs to compensate for the lack of oxygen and nutrients [13]. Thus, from the center of tumor region to its margin, the water content gradually decreases but is still higher than normal tissue. Therefore, at lower temperature, the indicated tumor area is small with the lower THz reflectance difference between tumor and normal tissues. Comparatively, with the increase of temperature, the tumor edge area is gradually shown in THz imaging due to the increase of water absorption coefficient [27].

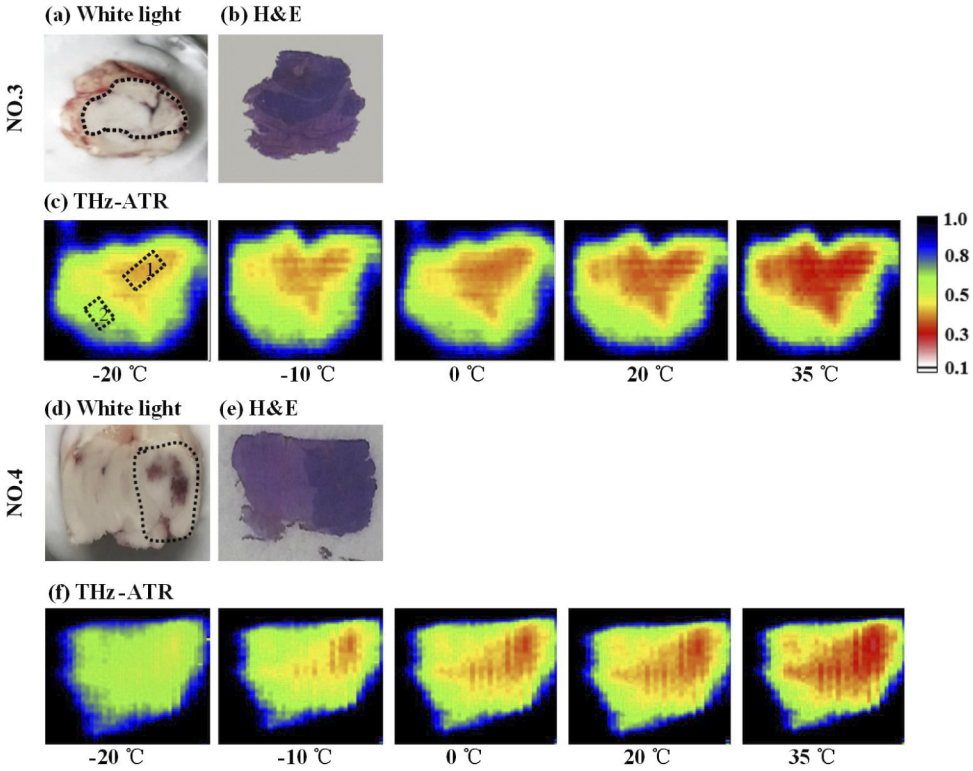

Fig. 4. (a) Visual, (b) H&E-stained and (c) THz-ATR images of glioma samples at temperature of -20 ℃ 35 ℃, the blue areas were the edge between sample and background. The red, green and black areas of (c) and (f) were the tumor tissue, normal tissue and background regions, respectively. The marked areas with dotted boxes 1 and 2 in (c) were the partial tumor and normal regions, respectively.

Figure 5 shows the averaged reflectivity (R_{ave}) of 5 samples in both tumor and normal regions, as the marked with dotted boxes 1 and 2 in Fig. 4 (c), respectively. The data was measured under the temperature interval of 5℃. For comparison, the averaged reflectivities of distilled water taken from THz-ATR image were also displayed. The R_{ave} in the tumor region was lower than that in the normal region. It indicates that the absorption of THz-wave in tumor tissue

Biomedical Optics EXPRESS

Table 1. Tumor sizes of H&E-stained image and THz-ATR images at different temperature

Mice NO.	Tumor sizes (mm^2)					
	H&E-stained image	THz-ATR images				
		T = - 20℃	T = - 10℃	T = 0℃	T = 20℃	T = 35℃
3	51.00	22.50	25.80	33.60	44.60	51.50
4	50.00	6.72	18.50	35.60	42.80	50.80

was higher than that in normal tissue. The trend of R_{ave} in tumor region was close to that in liquid water, which is deduced that THz radiation is responded mostly to the liquid water in tissues. In addition, the R_{ave} of tumor region with temperatures below 5℃ was decreased as the temperature increasing, which is owing to the fact that the water dehydration of sample with temperatures below 5℃ was low and the absorption coefficient of water was increased with temperature increasing [27]. On the contrary, the R_{ave} of tumor region with temperatures above 5℃ was slightly increased as the temperature increasing. The possible reason is that the water dehydration of sample with temperatures above 5℃ became relatively high and was increased with temperature increasing, whereas the absorption coefficient of water changes a little in the range of 5℃-35℃ [35]. In contrast to the tumor region, the R_{ave} of normal tissue was increased with the increase of temperature. This may be due to the refractive index of normal tissue at high temperature was higher than that at frozen temperatures [29,30]. Thus, the difference between tumor and normal tissues increases with the temperature. These results suggest that higher temperature was preferred for the THz imaging of brain glioma. Meanwhile, the R_{ave} of normal and tumor tissues at -10℃ were 44% ± 3% and 37% ± 3.2%, respectively. The R_{ave} of normal and tumor tissues at 20℃ were 53.4% ± 2.4% and 30% ± 2%, respectively. The difference value between tumor and normal tissues at -10℃ and 20℃ were 7% and 23.4%, respectively. According to the THz spectrum of freshly excised brain tissues based on THz-TDS system, the ATR reflectivity (R) can be calculated. For 2.52 THz, the calculated reflectivity of tumor and normal tissues using the average complex refractive indices of tissues are 92% and 89% at -10℃, and they are 56% and 26% at 20℃, respectively. Thus, the calculated difference value between tumor and normal tissues at -10℃ and 20℃ were 3% and 30%, respectively. These experimental results show good trends consisted with that in theoretical calculation. Although the calculation value based on THz spectrum were slightly different from that in experimental results, these can be attributed to the water dehydration during the processes of thin-sliced sample preparation and measurement. During the temperature dependent spectroscopy and imaging, the samples were measured by gradually increasing temperature, there was inevitable water loss and measurement error. The close contact of sample imaging surface with ATR window and measurement of multiple samples can reduce the error effectively. To sum up, THz spectroscopy and imaging of freshly excised brain tissues have demonstrated that the THz optical difference between tumor and normal tissues increased with the temperature increasing.

3.3. THz imaging of an in vivo mouse brain glioma model

Based on the difference between normal and tumor region of freshly excised brain tissues increased with temperature increasing in THz measurement, we tried to perform THz-ATR imaging of *in vivo* mouse brain glioma model, which can provide the basis for clinical application.

Figure 6 shows the visual *in vivo*, THz-ATR, visual *ex vivo* and H&E-stained images for brain tissues with (NO. 5 and NO. 6) and without (NO. 7) tumor samples. After the mice were anesthetized with 40 mg/kg pentobarbital by intraperitoneal injection, a cranial window was made and exposed the brain tissue. The surrounded blood and cerebrospinal fluid were sucked away by brain cotton slices. In Fig. 6 (a), the dark regions of mice brain in visual images were tumor regions. Then, the mouse brain was close contact to the bottom of prism for THz image.

Biomedical Optics EXPRESS

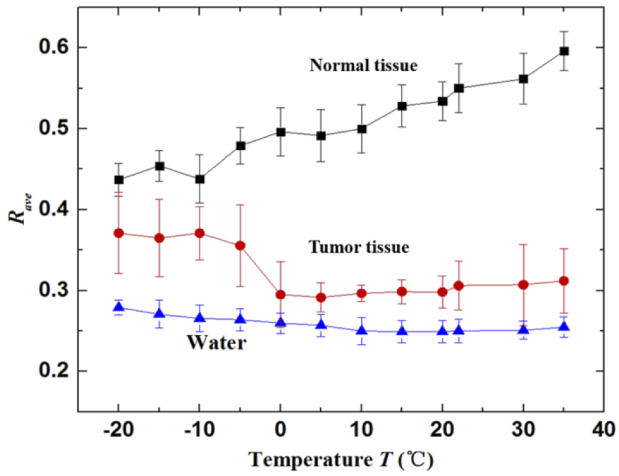

Fig. 5. The averaged reflectivity in the tumor tissue, normal tissue and distilled water at temperature interval of 5°C.

Figure 6 (b) shows the THz images of *in vivo* brain tissues with and without tumor based on THz-ATR imaging system. Each pixel was described using the R_r and a lower R_r mean the larger sample absorption. The high absorption regions of THz-wave were tumor regions, as shown in the red region in Fig. 6 (b). For the tumor tissue, the R_r values of the tumor regions was lower than 31%, whereas the R_r values for the normal tissues was rarely lower than 31%. Considering all the *in vivo* samples, the R_{ave} value of the tumor and normal tissues for brain tissues were $25\% \pm 6\%$ and $36\% \pm 5\%$, respectively. Thus, the threshold value of 31% was chosen to differentiate tumor region from normal tissue in Fig. 6(b). It was clearly seen that THz images of glioma mice showed obvious difference in tumor regions compared with the normal tissues, but the THz image for the normal mouse looks uniform, where the blue pixel around the center corresponded the needle were left over from image processing. The R_{ave} value of tumor regions in the THz imaging with tumor group was lower than that in the THz imaging with normal group. This can be attributed to the water content in the tumor region is higher than that in normal tissue. Compared with freshly excised brain tissue, the R_{ave} value of both tumor and normal tissues in *in vivo* brain tissue were lower. It could be because water dehydration during the processes of *ex vivo* brain tissue sample preparation and measurement. After the THz imaging, the whole brain was extracted from the mice and pathologically determined with the H&E-stained image, as shown in Fig. 6 (c) and (d). The tumor region appeared light-colour in the visible images of frozen samples, which was marked by dashed lines in Fig. 6 (c). In general, tumor regions in THz-ATR images were corresponding well with that in visible and H&E-stained images. The little position and size shifts for the sample can be attributed to the process of sample preparation, where the surfaces of the *in vivo* fresh tissue for THz image and H&E-stained sections were slightly different. Especially, it should be mentioned that, compared to our previous of in vivo glioma detection using THz reflection system [17], the ATR imaging has the advantages of high imaging contrast. Considering the orthotopic brain glioma in mice model used in our experiment agglutinates as a cluster, it cannot mimic the unclear margins and tissue heterogeneities, including necrosis, hemorrhage, and even microvascularity, that are usually inherent to human brain glioma. Therefore, further investigations with human tissue or alternative animal glioma model (like homograft glioma model 101.8 [14]) are necessary to evaluate the practicability of this method in clinical surgery.

Biomedical Optics EXPRESS

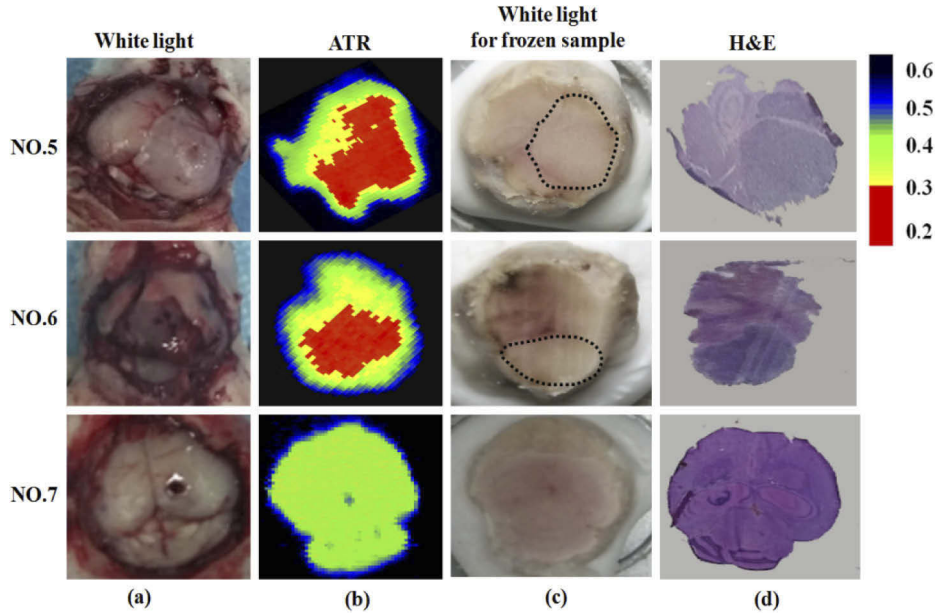

Fig. 6. (a) *In vivo* visual image, (b) THz wave total reflection image, (c) freezing visual image, and (d) H&E-stained image for NO. 5-7 samples, the blue areas were the edge between sample and background. The red, green and black areas of (b) were the tumor tissue, normal tissue and background regions, respectively.

4. Conclusions

The freshly *ex* vivo mice brain tissues with glioma were measured using THz spectroscopy and ATR imaging at different temperatures. The results show that the average values of refractive index and absorption in normal tissues were both smaller than that in tumor tissue at 20℃ and -10℃ in the range from 0.4 THz to 2.53 THz. In addition, appropriate sample temperature and THz frequency should be selected for better discriminating glioma from the normal tissue. Furthermore, the *in vivo* brain glioma regions can be differentiated clearly using THz-ATR imaging system. The high absorption region in THz images corresponded well with the tumor region in visible and H&E-stained images. Although additional studies are required, the temperature-dependent THz measurement technique used in this study holds great promise as a diagnostic tool for *ex vivo* and *in vivo* brain gliomas.

Funding. National Natural Science Foundation of China (61771332, 61775160, 62011540006, 62175182, U1837202).

Acknowledgements. This work was supported by the National Natural Science Foundation of China (Grant Nos. U1837202, 62175182, 61775160, 61771332, 62011540006).

Disclosures. The authors declare that there are no conflicts of interest related to this article.

Data Availability. Data underlying the results presented in this paper are not publicly available at this time but may be obtained from the authors upon reasonable request.

References

1. S. G. Liu, "Recent development of terahertz science and technology," China basic science **12**, 481–485 (2006).
2. K. Kawase, Y. Ogawa, Y. Watanabe, and H. Inoue, "Non-destructive terahertz imaging of illicit drugs using spectral fingerprints," Opt. Express **11**(20), 2549–2554 (2003).
3. G. J. Wilmink, "Invited review article: current state of research on biological effects of terahertz radiation," J Infrared Milli Terahz Waves **32**(10), 1074–1122 (2011).
4. R. M. Woodward, B. E. Cole, V. P. Wallace, R. J. Pye, D. D. Arnone, E. H. Linfield, and M. Pepper, "Terahertz pulse imaging in reflection geometry of human skin cancer and skin tissue," Phys. Med. Biol. **47**(21), 3853–3863 (2002).

Biomedical Optics EXPRESS

5. A. J. Fitzgerald and E. Al, "Terahertz pulsed imaging of human breast tumors," Radiology **239**(2), 533–540 (2006).
6. L. H. Eadie, C. B. Reid, A. J. Fitzgerald, and V. P. Wallace, "Optimizing multi-dimensional terahertz imaging analysis for colon cancer diagnosis," Expert Systems with Applications **40**(6), 2043–2050 (2013).
7. M. A. Brun, F. Formanek, A. Yasuda, M. Sekine, N. Ando, and Y. Eishii, "Terahertz imaging applied to cancer diagnosis," Phys. Med. Biol. **55**(16), 4615–4623 (2010).
8. Q. T. Ostrom, L. Bauchet, F. G. Davis, I. Deltour, J. L. Fisher, C. E. Langer, M. Pekmezci, J. A. Schwartzbaum, M. C. Turner, K. M. Walsh, M. R. Wrensch, and J. S. Barnholtz-Sloan, "The epidemiology of giloma in adults: a "state of the science review"," Neuro-Oncology **16**(7), 896–913 (2014).
9. M. Hefti, H. M. Mehdorn, I. Albert, and L. Dorner, "Fluorescence-guided surgery for malignant glioma: a review on aminolevulinic acid induced protoporphyrin IX photodynamic diagnostic in brain tumors," Curr. Med. Imaging Rev. **6**(4), 254–258 (2010).
10. K. Meng, T. Chen, T. Chen, L. Zhu, Q. Liu, Z. Li, F. Li, S. Zhong, Z. Li, H. Feng, and J. Zhao, "Terahertz pulsed spectroscopy of paraffin-embedded brain glioma," J. Biomed. Opt **19**(7), 077001 (2014).
11. S. Oh, S. Kim, Y. Ji, K. Jeong, Y. Park, J. Yang, D. Park, S. Noh, S. Kang, Y. Huh, J. Son, and J. Suh, "Study of freshly excised brain tissues using terahertz imaging," Biomed. Opt. Express **5**(8), 2837–2842 (2014).
12. S. Yamaguchi, Y. Fukushi, O. Kubota, T. Itsuji, T. Ouchi, and S. Yamamoto, "Origin and quantification of differences between normal and tumor tissues observed by terahertz spectroscopy," Phys. Med. Biol. **61**(18), 6808–6820 (2016).
13. S. Yamaguchi, Y. Fukushi, O. Kubota, T. Itsuji, T. Ouchi, and S. Yamamoto, "Brain tumor imaging of rat fresh tissue using terahertz spectroscopy," Sci. Rep. **6**(1), 30124 (2016).
14. A. Kucheryavenko, N. Chernomyrdin, A. Gavdush, A. Alekseeva, P. V. Nikitin, I. N. Dolganova, P. A. Karasik, A. S. Khalansky, I. E. Spektor, M. Skorobogatiy, V. V. Tuchin, and K. Zaytsev, "Terahertz dielectric spectroscopy and solid immersion microscopy of ex vivo glioma model 101.8: brain tissue heterogeneity," Biomed. Opt. Express **12**(8), 5272–5289 (2021).
15. N. V. Chernomyrdin, M. Skorobogatiy, A. A. Gavdush, G. R. Musina, G. M. Katyba, G. A. Komandin, A. M. Khorokhorov, I. E. Spektor, V. V. Tuchin, and K. I. Zaytsev, "Quantitative super-resolution solid immersion microscopy via refractive index profile reconstruction," Optica **8**(11), 1471–1480 (2021).
16. L. Wu, D. Xu, Y. Wang, Y. Zhang, H. Wang, B. Liao, S. Gong, T. Chen, N. Wu, H. Feng, and J. Yao, "Horizontal-scanning attenuated total reflection terahertz imaging for biological tissues," Neurophotonics **7**(2), 25005 (2020).
17. L. Wu, D. Xu, Y. Wang, B. Liao, Z. Jiang, L. Zhao, Z. Sun, N. Wu, T. Chen, H. Feng, and J. Yao, "Study of in vivo brain glioma in a mouse model using continuous-wave terahertz reflection imaging," Biomed. Opt. Express **10**(8), 3953–3962 (2019).
18. Y. B. Ji, S. J. Oh, S. G. Kang, J. Heo, S. H. Kim, Y. Choi, S. Song, H. Y. Son, S. H. Kim, J. H. Lee, S. J. Haam, Y. M. Huh, J. H. Chang, C. Joo, and J. S. Suh, "Terahertz reflectometry imaging for low- and high-grade gliomas," Sci. Rep. **6**(1), 36040 (2016).
19. G. M. Png, R. Flook, B. W.-H. Ng, and D. Abbott, "Terahertz spectroscopy of snap-frozen human brain tissue: an initial study," Electron. Lett. Iee The Institution of Engineering and Technology45(7), 343–345 (2009).
20. A. A. Gavdush, N. V. Chernomyrdin, K. M. Malakhov, S. T. Beshplav, I. N. Dolganova, A. V. Kosyrkova, P. V. Nikitin, G. R. Musina, G. M. Katyba, I. V. Reshetov, O. P. Cherkasova, G. A. Komandin, V. E. Karasik, A. A. Potapov, V. V. Tuchin, and K. I. Zaytsev, "Terahertz spectroscopy of gelatin-embedded human brain gliomas of different grades: a road toward intraoperative THz diagnosis," J. Biomed. Opt. **24**(02), 1–5 (2019).
21. A. A. Gavdush, N. V. Chernomyrdin, G. A. Komandin, I. N. Dolganova, P. V. Nikitin, G. R. Musina, G. M. Katyba, A. S. Kucheryavenko, I. V. Reshetov, A. A. Potapov, V. V. Tuchin, and K. I. Zaytsev, "Terahertz dielectric spectroscopy of human brain gliomas and intact tissues ex vivo: double-debye and double-overdamped-oscillator models of dielectric response," Biomed. Opt. Express **12**(1), 69–83 (2021).
22. P. Wesseling, J. Kros, and J. Jeuken, "The pathological diagnosis of diffuse gliomas: towards a smart synthesis of microscopic and molecular information in a multidisciplinary context," Diagnostic Histopathology **17**(11), 486–494 (2011).
23. C. S. Joseph, R. Patel, V. A. Neel, R. H. Giles, and Anna N. Yaroslavsky, "Imaging of ex vivo nonmelanoma skin cancers in the optical and terahertz spectral regions optical and terahertz skin cancers imaging," J. Biophotonics **7**(5), 295–303 (2014).
24. Y. Wang, Y. Wang, D. Xu, L. Wu, G. Wang, B. Jiang, T. Yu, C Chang, T. Chen, and J. Yao, "Interference elimination based on inversion method for continuous-wave terahertz reflection imaging," Opt. Express **28**(15), 21926–21939 (2020).
25. M. Khanmohammadi, A. Garmarudi, K. Ghasemi, H. Jaliseh, and A. Kaviani, "Diagnosis of colon cancer by attenuated total reflectance-Fourier transform infrared microspectroscopy and soft independent modeling of class analogy," Med Oncol **26**(3), 292–297 (2009).
26. Y. Wang, G. Wang, D. Xu, B. Jiang, M. Ge, L. Wu, C. Yang, N. Mu, S. Wang, C. Chang, T. Chen, H. Feng, and J. Yao, "Terahertz spectroscopic diagnosis of early blast-induced traumatic brain injury in rats," Biomed. Opt. Express **11**(8), 4085–4098 (2020).
27. O. S. Jae, J. Kang, M. Inhee, S. Jin-Suck, H. Yong-Min, H. Seungjoo, and S. Joo-Hiuk, "Nanoparticle-enabled terahertz imaging for cancer diagnosis," Opt. Express **17**(5), 3469–3475 (2009).
28. J. Park, H. Choi, H. Cheon, S. Cho, and J. Son, "Terahertz imaging of metastatic lymph nodes using spectroscopic integration technique," Biomed. Opt. Express **8**(2), 1122–1129 (2017).

Biomedical Optics EXPRESS

29. Y. C. Sim, K.-M. Ahn, J. Y. Park, C. S. Park, and J.-H. Son, "Temperature-dependent terahertz imaging of excised oral malignant melanoma," IEEE J. Biomed. Health Inform. **17**(4), 779–784 (2013).
30. Y. C. Sim, J. Y. Park, K.-M. Ahn, C. Park, and J.-H. Son, "Terahertz imaging of excised oral cancer at frozen temperature," Biomed. Opt. Express **4**(8), 1413–1421 (2013).
31. A. K. Zotov, A. A. Gavdush, G. M. Katyba, L. P. Safonova, N. V. Chernomyrdin, and I. N. Dolganova, "In situ terahertz monitoring of an ice ball formation during tissue cryosurgery: a feasibility test," J. Biomed. Opt. **26**, 1 (2021).
32. L. M. Wu, D.G. Xu, Y. Y. Wang, M. L. Ge, H. B. Li, Z. L. Wang, and J. Q. Yao, "Common path continuous terahertz reflection and attenuated total reflection imaging," Acta Phys. Sin. **70**(11), 118701 (2021).
33. R. R. Edelman, J. R. Hesselink, and M. B. Zlatkin, *Clinical Magnetic Resonance Imaging*, Chap. 1 (Saunders, 1996).
34. H. R. Zelsmann, "Temperature dependence of the optical constants for liquid H_2O and D_2O in the far IR region," J. Mol. Struct. **350**(2), 95–114 (1995).
35. H. Yada, M. Nagai, and K. Tanaka, "Origin of the fast relaxation component of water and heavy water revealed by terahertz time-domain attenuated total reflection spectroscopy," Chem. Phys. Lett. **464**(4-6), 166–170 (2008).